Multimodal biomechanical methods supporting abdominal aortic aneurysm management

Róbert Nagy, Imre Bojtár

Department of Structural Mechanics, Faculty of Civil Engineering, Budapest University of Technology and Economics

robert.nagy@mail.bme.hu

Abstract

In clinical practice, management of abdominal aortic aneurysms (AAA) is predominantly based on the diameter of the lumen. State-of-the-art fluid structure interaction (FSI) simulations have proven to be superior in estimating rupture risk, although they still have considerable shortcomings. In this paper we address one such unresolved problem, and present the outline of biomechanical material parameter distribution identification via inverse finite element (FE) analysis. Our method is based on the non invasive approximation of the displacement field using electrocardiogram-gated computer tomography angiography (ECG-gated CT-angiography, CTA) and estimating the load field with usual computational fluid dynamics (CFD) simulations. Parameters of our model connecting the two abovementioned sets of variables result from an optimization algorithm minimizing a work and energy related variational functional. Consequently, also supported by experimental measurements, we are able to assess local distribution of the biomechanical material properties of the arterial wall and give a functional characterization of vessel wall degeneration.

Keywords: abdominal aortic aneurysm, risk of rupture, in vivo measurement, biomechanical material parameters, ECG-gated CTA, clinical application

1. Introduction

In healthy elderly men, the diameter of the infrarenal abdominal aorta ranges between 15 mm and 24 mm.[1] Abdominal aortic aneurysm (AAA) is a persistent and irreversible, circumscribed, spindle-shaped dilatation of the vessel with diameters exceeding 1.5 times this value.[2,3] Ensuing rupture of these lesions is extremely hazardous, with lethal outcomes in the overwhelming majority of the cases.[4,5] Since the advent of modern imaging technologies and regular screening tests, aortic deformations are often discovered at an early stage, and although, elective repair by open surgery or endovascular stent grafting at this point can decrease mortality ratio significantly, treatment of these lesions remains a high risk procedure.[6]

Therefore, any prediction rule regarding the risk of rupture is of paramount importance.

2. Motivation

In clinical practice, the management of asymptomatic aortic aneurysms is predominantly based on the measurement of maximal lumen diameter and its rate of expansion with critical values being 5.5 cm and 1 cm/year, respectively.[7] Although, a strong correlation has been observed, that also can be well explained by Laplace's law of thin membranes; there is no exclusive causal relation between these factors and the probability of rupture.

Insufficient effectiveness of early elective surgical repair[8] and the still occurring rupture

of untreated small aneurysms (dilatations less than 5.5 cm in diameter)[9] raised the demand of an improved decision strategy based on biomechanical concepts: rupture occurs when the blood flow induced stress of the vessel wall reaches the strength limit of the tissue. Patient-specific numerical modeling techniques adopting this concept[10-14] are proven to have higher discriminatory value, with a proper reproducibility,[15] than the maximal diameter.

These methods handle the liquid blood and the solid wall phases separately by solving the respective differential equations in a fully coupled fluid-structure interaction (FSI) algorithm. In practice, first, the geometry of the lumen is captured at a single timestep with CTA imaging; the blood pressure is measured usually on the arm, and then transformed to transient volumetric flow rate inlet and pressure outlet boundary conditions for the examined segment using the method of characteristics on a one-dimensional branching model.[16] With an adequate fluid model for the blood, the CFD calculation yields the pressure acting on the wall as the boundary condition for the FE model, which itself is embedded in an elastic support environment. Conversely, the displacement field resulting from the FE model of the solid phase augments the boundary condition for the CFD simulation of the liquid phase. This concept requires an iteration algorithm in each timestep of an unsteady problem until the dynamic equilibrium is fulfilled.

One of the greatest shortcomings of these methods – beside the complex support boundary conditions[17] – is the lack of individual calibration of the material parameters of the wall. Their distribution has a significant impact[18,19] on the stress distribution and on the rupture criterion as well. In concordance with clinical observations, at the dilated part local stiffening of the hyperstatic structure concentrates the stresses exactly where the resistance decreased.

3. Purpose

Our aim is to develop a new, non invasive method to measure material parameters in vivo; thus, analyzing the adequacy of the wall stresses calculated by existing methods, and completing the characterization of the aneurysm with the assessment of tissue degeneration. The procedure involves 5 cornerstones: (1) displacement field determination, (2) corresponding load field calculation, (3) identification of local material model parameters, (4) assessment of vessel wall degeneration, and (5) the validation of the methodology. In the following, we present the basic ideas behind these steps.

4. Method

4.1. Determination of the displacement field

Characterizing the dynamic movement of the living tissue is possible in theory by following either natural landmarks or artificial markers.[20] The first requires a sophisticated experimental setup, while the second is highly invasive, both of which we want to avoid. Our method stems from the novel application of the electrocardiogram-gated computer tomography angiography (ECG-gated CTA) – commonly used in cardiology – opening new horizons for investigation of the dynamic behavior of the artery in contrast to the more commonly used static properties.[21]

Image acquisition

We used a Philips Brilliance iCT (Koninklijke Philips NV, Best, Netherlands) device to scan the aorta with slice thickness of 1 mm and transverse voxel size of approximately 0.5 mm. The reconstruction was performed at 10 discrete timesteps of the R-R interval with an active contour algorithm. The total displacement amplitude of a point of interest at the aortic

wall was comparable to the estimated measurement precision (identified by the voxel size in the transverse direction).

Parametric surface representation

At each timestep we constructed a parametric bicubic spline surface of the arterial lumen by minimizing the smoothness measure of the surface under the condition that the deviation of the measured points from the fitted surface exceeds the estimated measurement error (identified by the voxel size in the transverse direction) with probability less than a given significance level. The motion tracking of the resulting surface point is an ill-posed problem, since we have no information on the in-plane displacements. Two approaches are at hand: The first is solving the weak formulation of the problem by minimizing an image similarity measure combined with the variational functional of the mechanical energy. The second – which is followed in this paper due to its numerical efficiency and the advantage of restricting the problem to geometric properties

– is to amend the local, strong formulation by making auxiliary constraint on the movement. Based on FSI simulation observations, we assume the incremental displacement vector of the reference surface to align with its corrected normal vector. The correction accounts for the periodic movement and plays the role as the measure of the assumption efficiency. As *Figure 1* shows, the necessary correction decreases with increasing temporal resolution.

Isogeometric analysis

The idea of using the functions describing the geometry as basis functions of the finite element analysis was introduced by Hughes et al.[22] and summarized by Cottrell et al.[23] applying the non-uniform rational B-spline (NURBS) description within the isogeometric paradigm to close the gap between CAD based design and analysis not requiring the intermediate step of mesh generation and enabling the work on the exact geometry. This approach is adopted in our investigations so that the control point motion function defines the kine-
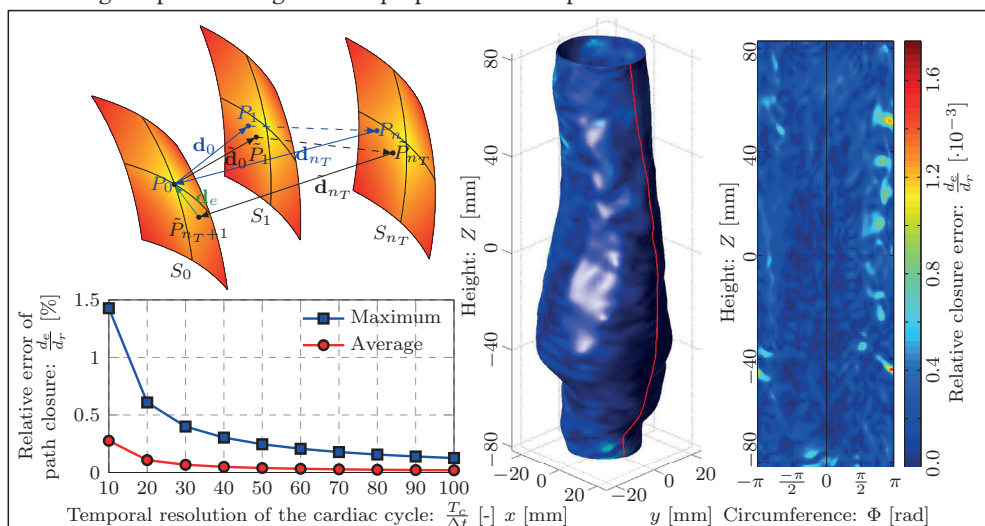
Figure 1. The top left figure shows the surface normal vectors (black), the remaining closure error (green) after a period, and the displacement increments (blue). The bottom left figure shows the maximum and average closure error convergence with increasing temporal resolution. The spatial distribution of the error in the converged state is presented on the right
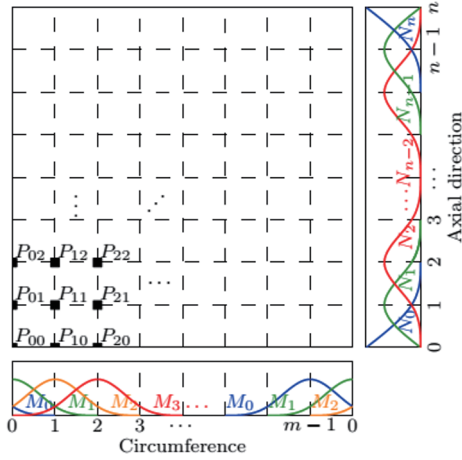
Figure 2. Natural and periodic univariate cubic uniform basis function constituting the bicubic uniform spline, the parameter mesh and the P_{ij} control point values
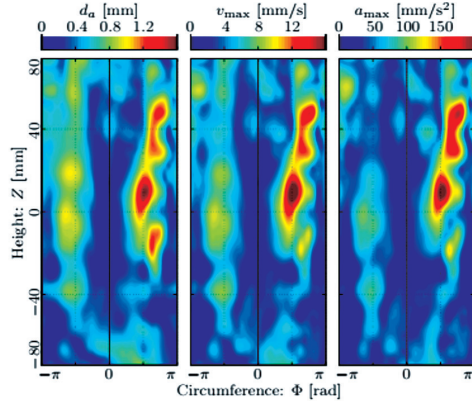

Figure 3. Amplitudes of the kinematic variables in a cardiac cycle. The sides move with displacement amplitude approximately 1 mm, while the frontal dilated part virtually remains in place
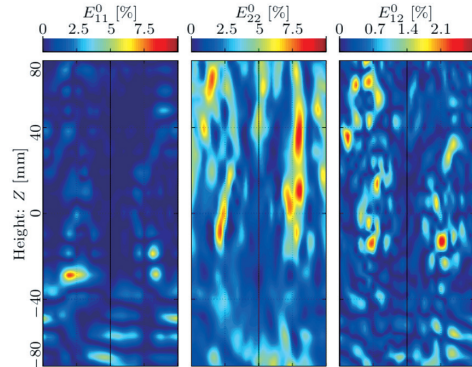
matics of the structure with the given set of basis functions as demonstrated in *Figure 2*.

The reference surface motion function (χ) is consequently defined in the form of (1), where ξ^1, $\xi^2 \in \Omega$ are the surface parameters, N_i, M_j are the basis functions, t is the time and T_c is the duration of the heartbeat. The velocity and acceleration – components that are also needed in future dynamic analysis – are easily derived by partial differentiation. The displacement amplitude and the maximal velocity and acceleration magnitudes are shown in *Figure 3*.

$$\chi\left(\xi^1,\xi^2,t\right)=\sum_{j=1}^{n_1}\sum_{i=1}^{n_2}N_i^p\left(\xi^1\right)M_j^q\left(\xi^2\right)\mathbf{W}_{ij}\left(t\right),$$

$$\mathbf{W}_{ij}\left(t\right)=\mathbf{W}_{ij0}^A+\sum_{k=1}^{n_f}\mathbf{W}_{ijk}^A\cos(\frac{2\pi k}{T_c}t)+\mathbf{W}_{ijk}^B\sin(\frac{2\pi k}{T_c}t). \tag{1}$$

Figure 4 shows the amplitudes of the in-plane Green-Lagrange strain components in local orthonormal coordinate system at the reference surface. These values oscillate around the initial strain, which is approximately 0.3.[24-26]

Figure 4. Green-Lagrange strain amplitude components at the lumen

The main load bearing direction is the circumferential one (E_{22}) with peak strain amplitude values of 0.1 surrounding the bulge region, while the values of strain amplitude are with an order of magnitude smaller within this region. This fact squares well with the expected behavior of a stiffer inclusion, and is also supported by observations of rupture, mostly occurring at the dilated part by having small

strains in a weakened region and high values at its border with a thin transition zone. In-plane shear (E_{12}) behaves similarly with peak values around 3%. Axial stretch (E_{11}) is also small at the dilatation and large at locations of high axial curvature.

Material point kinematics

In this example only the inner side of the arterial wall was extracted from the images, in order to characterize the rotational displacement of the material points situated above this reference surface, since it was convenient to suppose that the directors (straight material lines normal to the initial reference surface) remain straight and normal to the deformed lumen throughout the whole process, leading to Kirchhoff-Love shell theory. It is possible to determine the displacement field of the outer surface of the wall, as well, in a similar manner, which provides the linear approximation of the deflection of the director from the surface normal, which accommodates the transverse shear deformations using the Reissner-Mindlin shell formulation.

4.2. Determination of the load field

Simultaneously with the geometry scan, over-pressure and velocity profile measurements were carried out at a limb, which was then transformed to the desired aortic section via a 1D systematic model – analogous to the electric circuit model – serving as boundary condition for the fluid simulation.[16] The previously determined wall displacement served as a moving wall boundary making the resource consuming FSI calculation unnecessary, which is an advantage of our model in terms of real-time applicability. The simulation was carried out within the ANSYS framework yielding the flow induced pressure and wall shear stress distribution acting on the wall.

4.3. Identification of local material model parameters

The power of these forces should be equal to the time derivative of the sum of the strain energy and kinetic energy. The power is calculated from the loads and the reference surface velocity function. The kinetic energy is given by the shell model and the reference surface velocity function, while for the estimate of strain energy we needed additional characteristics of the material model, for which well developed formulae were found in the literature based on a microstructural approach.[27] Model parameter identification was carried out by a fast Levenberg-Marquardt local optimization algorithm where the objective function gradient is provided numerically in time comparable to a normal function evaluation by virtue of the local support property of the spline basis functions.
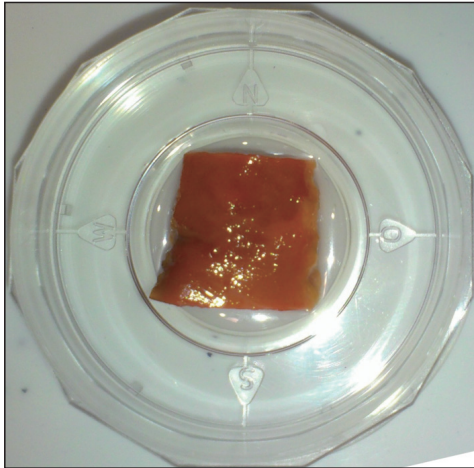
4.4. Degree of vessel wall degeneration

Changes in material properties will usually be accompanied by slow, gradual distension of vessel geometry. This phenomenon can be observed both on the macro- (stiffening) and microscale (decreased elastin content). We related the identified model parameters to these observed phenomena in order to get a threshold of material strength and to determine the level of degenerative process.

Aneurysmal aortic sections were dissected (see *Figure 5*) from patients undergoing to open surgery at the Heart and Vascular Center of Semmelweis University, where ECG-gated CTA images were also taken preceding the operations.
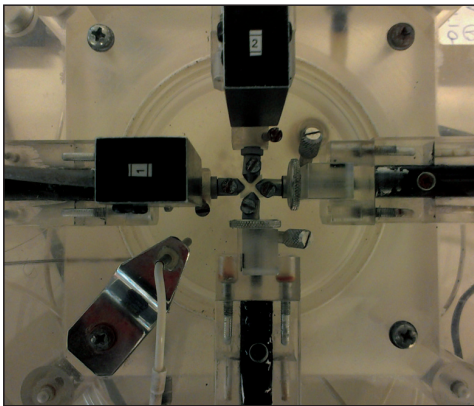
We measured macroscopic elastic behavior of the specimen by using displacement controlled equi-biaxial tensile tests shown in *Figure 6*,

while the microstructure of the same samples was assessed by multi-photon microscopy, which is capable to visualize collagen throughout the cross-section of arterial constitutive layers, as shown in *Figure 7*. Then, we stacked image slices together in order to get 3D data, and by the aid of an automatic image processing algorithm we were able to determine the collagen content and the distribution function

of the fiber orientation by applying a 3D Fourier transform.

4.5. Validation and verification

The applicability of the method components should be validated individually. The hypothesis of the displacement to be aligned with the corrected actual normal is observed by FSI simulations on geometries with small changes in curvature with homogenous hyperelastic material model. Deviations are expected at locations with negative Gaussian curvature. Experimental verification is also needed and proposed in the near future by natural landmark tracking. The load field determination procedure is documented extensively in the literature.[17] The material identification procedure carried out on noisy data is an optimization problem of well described approximating solution algorithms as well. To verify the process itself, in silico measurements of an artificial silicon artery loaded with pulsatile fluid flow are also planned.

Figure 5. Dissected aneurysm sample (Semmelweis University, Heart and Vascular Center)
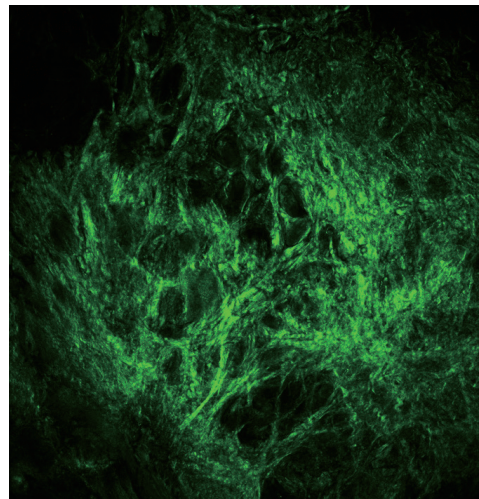

Figure 6. Equipment for equibiaxial tensile testing aneurysm specimens (Semmelweis University, Department of Biophysics and Radiation Biology Institute of Human Physiology and Clinical Experimental Research)

Figure 7. Dissected aneurysm sample (Semmelweis University, Heart and Vascular Center)

REFERENCES

1. *Liddington MI, Heather BP.* The relationship between aortic diameter and body habitus. European Journal of Vascular Surgery 1992;6:89-9.

2. *McGregor JC, Pollock JG, Anton HC.* The value of ultrasonography in the diagnosis of abdominal aortic aneurysm. Scottish Medical Journal 1975;20:133-7.

3. *Johnston KW, Rutherford RB, Tilson MD, Shah DM, Hollier L, Stanley JC.* Suggested standards for reporting on arterial aneurysms. Subcommittee on Reporting Standards for Arterial Aneurysms, Ad Hoc Committee on Reporting Standards, Society for Vascular Surgery and North American Chapter, International Society for Cardiovascular Surgery. Journal of Vascular Surgery 1991;13:452-8.

4. *Ingoldby CJ, Wujanto R, Mitchell JE, Epstein DM, Sculpher MJ, Greenhalgh RM.* Impact of vascular surgery on community mortality from ruptured aortic aneurysms. The British Journal of Surgery 1986;360:551-3.

5. *Kantonen I, Lepantalo M, Brommels M, Luther M, Salenius JP, Ylonen, the Finnvasc Study Group et al.* Mortality in ruptured abdominal aortic aneurysms. European journal of vascular and endovascular surgery 1999;17(3):208-12.

6. *Brown LC, Powell JT, Thompson SG.* The UK EndoVascular Aneurysm Repair (EVAR) trials: randomised trials of EVAR versus standard therapy. Health Technology Assessment 2012;16(9):1-218.

7. *Hirsch AT, Haskal ZJ, Hertzer NR, Bakal CW, Creager MA, Halperin JL, et al.* ACC/AHA 2005 Guidelines for the management of patients with peripheral arterial disease (lower extremity, renal, mesenteric, and abdominal aortic). Journal of the American College of Cardiology 2006;47(6):1239-312.

8. *Powell J.* Final 12-year follow-up of surgery versus surveillance in the UK small aneurysm trial. British Journal of Surgery 2007;94:6.

9. *Brewstera DC, Cronenwett JL, Hallett Jr. JW, Johnston KW, Krupski WC, Matsumura J.* Guidelines for the treatment of abdominal aortic aneurysms: Report of a subcommittee of the joint council of the American Association for Vascular Surgery and Society for Vascular Surgery. Journal of Vascular Surgery 2003;37(5):1106-17.

10. *Raghavan ML, Webster MW, Vorp DA.* Ex vivo biomechanical behavior of abdominal aortic aneurysm: assessment using a new mathematical model. Annals of Biomedical Engineering 1996;24(5):573-82.

11. *Raghavan ML, Vorp DA, Federle MP, Makaroun MS, Webster MW.* Wall stress distribution on three-dimensionally reconstructed models of human abdominal aortic aneurysm. Journal of Vascular Surgery 2000;31(4):760-9.

12. *Raghavan ML, Fillinger MF, Marra SP, Naegelein BP, Kennedy FE.* Automated methodology for determination of stress distribution in human abdominal aortic aneurysm. Journal of Biomechanical Engineering 2005;127(5):868-71.

13. *Fillinger MF, Raghavan ML, Marra SP, Cronenwett JL, Kennedy FE.* In vivo analysis of mechanical wall stress and abdominal aortic aneurysm rupture risk. Journal of Vascular Surgery 2002;36(3):589-97.

14. *Fillinger MF, Marra SP, Raghavan ML, Kennedy FE.* Prediction of rupture risk in abdominal aortic aneurysm during observation: Wall stress versus diameter. Journal of Vascular Surgery 2003;37(4):724-32.

15. *Hyhlik-Dürr A, Krieger T, Geisbüsch P, Kotelis D, Able T, Böckler D.* Reproducibility of deriving parameters of AAA rupture risk from patient-specific 3D finite element models. Journal of Endovascular Therapy 2011;18(3):289-98.

16. *Bárdossy G, Halász G.* Modeling blood flow in the arterial system. Periodica Polytechnica 2011;55:49-55.

17. *Józsa TI, Paál G.* Boundary conditions for flow simulations of abdominal aortic aneurysms, International Journal of Heat and Fluid Flow 2014;50:342-51.

18. *Speelman L, Bohra A, Bosboom EMH, Schurink, GWH, van de Vosse FN, Makaroun MS, Vorp DA.* Effects of wall calcifications in patient-specific wall stress analyses of abdominal aortic aneurysms. Journal of Biomechanical Engineering 2007;129(1):105-9.

19. *Li ZY, U-King-Im J, Tang TY, Soh E, See TC, Gillard JH.* Impact of calcification and intraluminal thrombus on the computed wall stresses of abdominal aortic aneurysm. Journal of Vascular Surgery 2008;47(5):928-35.

20. *Rausch MK, Bothe W, Kvitting JPE, Göktepe S, Craig Miller D, Kuhl E.* In vivo dynamic strains of the ovine anterior mitral valve leaflet. Journal of Biomechanics 2011;44(6):1149-57.

21. *Nagy R, Csobay-Novák Cs, Lovas A, Sótonyi P, Bojtár I.* Non invasive in vivo measurement of strain in human abdominal aortic aneurysms. Towards a novel approach to rupture risk estimation. Journal of Biomechanics 2015;48(10): 1876-86.

22. *Hughes TJR, Cottrell JA, Bazilevs Y.* Isogeometric analysis: CAD, finite elements, NURBS, exact geometry and mesh refinement. Computer methods in applied mechanics and engineering 2005;194(39):4135-95.

23. *Cottrell JA, Hughes TJR, Bazilevs Y.* Isogeometric Analysis: Toward Integration of CAD and FEA. John Wiley&Sons 2009, ISBN 978-0-470-74873-2.

24. *Holzapfel GA, Sommer G, Auer M, Regitnig P, Ogden RW.* Layer specific 3d residual deformations of human aortas with non-atherosclerotic intimal thickening. Annals of biomedical engineering 2007;35:530-45.

25. *Langewouters G, Wesseling K, Goedhard W.* The static elastic properties of 45 human thoracic and 20 abdominal aortas in vitro and the parameters of a new model. Journal of biomechanics 1984;17:425-35.

26. *Stålhand J, Klarbring A.* Aorta in vivo parameter identification using an axial force constraint. Biomechanics and modeling in mechanobiology 2005;3:191-9.

27. *Holzapfel GA, Gasser TA, Ogden RW.* A new constitutive framework for arterial wall mechanics and a comparative study of material models. J Elasticity, 2000;61:1-48.

Róbert Nagy
Department of Structural Mechanics, Faculty of Civil Engineering, Budapest University of Technology and Economics
H-1111 Budapest, Műegyetem rkp. 3. K building, KM 63.
Tel.: (+36) 1 463-1434